

1 **Fast turnover of genome transcription across evolutionary time exposes entire**
2 **non-coding DNA to *de novo* gene emergence**

3

4 Rafik Neme and Diethard Tautz

5 Max-Planck Institute for Evolutionary Biology

6 August-Thienemann Strasse 2

7 24306 Plön, Germany

8

9 email: tautz@evolbio.mpg.de

10

11

12 **Abstract**

13 **Deep sequencing analyses have shown that a large fraction of genomes is transcribed, but the significance of**
14 **this transcription is much debated. Here, we characterize the phylogenetic turnover of poly-adenylated**
15 **transcripts in a comprehensive sampling of taxa of the mouse (genus *Mus*), spanning a phylogenetic distance of**
16 **10 Myr. Using deep RNA sequencing we find that at a given sequencing depth transcriptome coverage becomes**
17 **saturated within a taxon, but keeps extending when compared between taxa, even at this very shallow**
18 **phylogenetic level. Our data show a high turnover of transcriptional states between taxa and that no major**
19 **transcript-free islands exist across evolutionary time. This suggests that the entire genome can be transcribed**
20 **into poly-adenylated RNA when viewed at an evolutionary time scale. We conclude that any part of the non-**
21 **coding genome can potentially become subject to evolutionary functionalization via *de novo* gene evolution**
22 **within relatively short evolutionary time spans.**

23

24

25 **Introduction**

26 Genome-wide surveys have provided evidence for "pervasive transcription", i.e., much larger portions of the
27 genome are transcribed than would have been predicted from annotated exons (Clark et al. 2011; Hangauer et al.
28 2013; Kellis et al. 2014). Most are expected to be non-coding RNAs (lncRNAs) of which some have been shown to
29 be functional. However, the general conservation level of these additional transcripts tends to be low, which raises
30 the question of their evolutionary turnover dynamics (Kutter et al. 2012; Kapusta and Feschotte 2014). They are
31 currently receiving additional attention, since they could be a source for *de novo* gene formation via a proto-gene
32 stage (Carvunis et al. 2012; Ruiz-Orera et al. 2014, Neme and Tautz 2014). It has been shown that *de novo* gene
33 emergence shows particularly high rates in the youngest lineages (Tautz and Domazet-Loaso 2011), indicating that
34 there is high turnover of such transcripts and genes between closely related species. Indeed, comparative studies

35 of *de novo* genes between *Drosophila* species (Palmieri et al. 2014) and within *Drosophila* populations (Zhao et al.
36 2014) have confirmed this.

37
38 A number of possibilities have been discussed by which new transcripts are generated in previously non-coding
39 regions, including single mutational events, stabilization of bi-directional transcription and insertion of
40 transposable elements with promotor activity (Brosius 2005; Gotea et al. 2013, Neme and Tautz 2013; Wu and
41 Sharp 2013; Sundaram et al. 2014; Ruiz-Orera et al. 2015). Detailed analyses of specific cases of emergence of a *de*
42 *novo* gene have shown that single step mutations can be sufficient to generate a stable transcript in a region that
43 was previously not transcribed and translated (Heinen et al. 2009; Knowles et al. 2009). The unequivocal
44 identification of *de novo* transcript emergence can only be made in a comparison between very closely related
45 evolutionary lineages, where orthologous genomic regions can be fully aligned, even for the neutrally evolving
46 parts of the genome (Tautz et al. 2013). While the available genome and transcriptome data for mammals and
47 insects are sufficient to screen for specific cases of *de novo* transcript emergence, they are still too far apart of
48 each other to allow a comprehensive genome-wide assessment. Our analysis here is therefore based on a new
49 dataset that reflects a very shallow divergence time-frame for relatives of the house mouse (*Mus musculus*).

50 51 **Results**

52 We selected populations, subspecies and species with increasing phylogenetic distance to the *Mus musculus*
53 reference sequence (Keane et al. 2011). This reference was derived from an inbred strain of the subspecies *Mus*
54 *musculus domesticus* and we use samples from three wild type populations of *M. m. domesticus* as the most
55 closely related taxa, separated from each other by about 3,000-10,000 years. Further, we use samples from the
56 related subspecies *M. m. musculus* and *M. m. castaneus*, which are separated since 0.3-0.5 million years. The other
57 samples are recognized separate species with increasing evolutionary distances (Figure 1). We call this set of
58 populations, subspecies and species collectively "taxa" in the following. Altogether they span 10 million years of
59 divergence, which corresponds to an average of 6% nucleotide difference for the most distant comparisons.

60
61 We obtained genome sequence reads for all taxa and mapped them to the mouse reference genome, using an
62 algorithm that was specifically designed to deal efficiently with problems that occur in cross-mapping between
63 diverged genomes (Sedlazeck et al. 2013; see Appendix 1 for validation). All regions that could be unequivocally
64 mapped for all taxa were then used for further analysis. We refer to this as the "common genome" which allows
65 comparisons on those regions of the genomes which have not been gained or lost along the phylogeny, i.e., are
66 common across all taxa (Figure 1–figure supplement 1). It represents 71.7% of the total reference genome length
67 (Figure 1–figure supplement 2). Hence, we are nominally not analyzing about a third of the total genome length,
68 but this corresponds to the highly repetitive parts for which unique and reliable mapping of transcriptomic reads

69 would not be possible. Also, changes in transcription derived from gain or loss of genomic regions do not
70 contribute to the patterns described below.

71

72 We chose three tissues for transcriptome sequencing, including testis, brain and liver. Previous studies had shown
73 that testis and brain harbor the largest diversity of transcripts (Necsulea and Kaessmann 2014). We sequenced
74 only the poly-A⁺ fraction of the RNA, i.e., our focus is on coding and non-coding exons in processed RNA.

75

76 We use non-overlapping sliding windows of 200nt to assay for presence or absence of reads within the windows
77 and express overall coverage as the fraction of windows showing transcription (see methods for details). We use
78 only uniquely mapping reads, implying that we neglect the contributions and dynamics at repetitive loci. We
79 display three thresholds of window coverage, the minimum being coverage by at least a single read, while the
80 higher ones represent at least 10 and 100 reads respectively. The first serves as a very inclusive metric of low-level
81 transcription, with the drawback of potentially including noise into the analysis, due to stochasticity in sampling,
82 while the others represent thresholds for more abundant transcripts that are unlikely to be affected by sampling
83 noise.

84

85 Among the three tissues analyzed, liver has the lowest overall read coverage while brain and testis have similar
86 overall levels (Figure 2A-C). Combining the data from all three tissues or triplicating the read depth for one tissue
87 (brain) increases the overall coverage in a similar way (Figure 2D, E).

88

89 Figure 2F shows the total coverage across all tissues and all sequencing runs, which amounts to an average of 50.0
90 \pm 2.5% per taxon. Hence, For each tissue, as well as in this combined set, we observe a very similar coverage in all
91 taxa, with only a slight increase in the low expressed fraction for the most distant comparisons (see also legend
92 Figure 2). This more or less stable pattern across phylogenetic time could either be due to the same regions being
93 transcribed in all taxa, or a more or less constant rate of turnover of gain and loss of transcription between taxa.

94

95 To test these alternatives, we have asked which part of the transcribed window coverage is shared between the
96 taxa and which is specific to the taxa. For this, we consider three classes: i) windows that are found in a single
97 taxon only, ii) windows that are found in 2-9 taxa, i.e. more than one but not in all and iii) windows shared among
98 all taxa (Figure 3; Figure 3–figure supplement 1 shows an extended version where class ii) is separated into each
99 individual group). However, such an analysis could potentially be subject to a sampling problem, i.e. not finding a
100 transcript in a taxon does not necessarily imply true absence, but could also be due to failure of sampling. This
101 would be particularly problematic for singleton reads, since the probability of falsely not detecting one in a second
102 sample that expresses it at the same level is about 37%. However, given that we ask whether it is detected in any

103 of the other 9 taxa, the probability of falsely not detecting it if it exists across all of them becomes small (0.01%)
104 (see also further analysis on singletons below).

105

106 Between 1-7% of transcribed windows are unique to one taxon only, with the more distant taxa showing the
107 higher percentages (Figure 3). Most of these taxon-specific transcripts are lowly expressed (< 10 reads per
108 window), but the more distant taxa (MAT and APO in Figure 3 I,J) show also some more highly expressed ones. We
109 find a total of 6,566 windows with read counts >50 that occur in a single taxon only, mostly in the long branches
110 leading to MAT (1,638 windows) and APO (4,485 windows), but some also between the most closely related taxa
111 (43 windows for DOM, including populations; 38 windows for MUS, including populations).

112

113 Approximately 18% of windows show transcripts shared across all taxa. These include most of the very highly
114 expressed ones (>100 reads per window), but also a fraction of the low expressed ones (Figure 3). They are also
115 enriched in annotated genes, especially in exons of protein coding genes, but also in non-coding genes (Figure 3-
116 figure supplement 2). The class ii) windows (sharing between 2-9 taxa in Figure 3) represents the genes showing
117 more or less turnover between taxa, with more turnover the more distant they are of each other (Figure 3-figure
118 supplement 1). This class constitutes cumulatively the largest fraction (between 26-33% of whole genome
119 coverage - Figure 3), supporting the notion of a fast turnover of most of the transcribed regions between taxa.

120

121 The taxon-specific turnover of transcripts is also reflected in a distance tree of shared coverage. Taxa that are
122 phylogenetically closer to each other share more transcripts, i.e. the tree topology mimics that of a phylogenetic
123 tree based on molecular sequence divergence (Figure 4A,B). This implies that the turnover of the transcripts is not
124 random, but time dependent, i.e. more closely related taxa share more transcripts. However, the relative branch
125 lengths are much extended for the more closely related taxa compared to the molecular distances, implying that
126 there is a particularly high turnover between them.

127

128 To assess in how much this could be due a sampling variance problem at low expression levels, we have separately
129 analyzed the transcripts that are represented by single reads only, since these should be most sensitive towards
130 sampling problems. Depending on read depth and tissue, they constitute about 2-12% of the common windows
131 when assessed on a per sample basis (Figure 4 - figure supplement 1). However, most of these singletons in a given
132 sample were re-detected in another tissue or another taxon (Figure 4 - figure supplement 1), such that less than
133 2% are present in a given taxon (Figure 4 - figure supplement 1) and less than 7% cumulatively throughout the
134 whole dataset (Figure 4 - figure supplement 2). We used the extended brain sample reads, split them into three
135 non-overlapping sets of about 100 Mill reads for each taxon and constructed trees out of these sets using only the
136 singleton reads. This is the equivalent of repeating the same experiment three times. We find indeed differences in
137 the resulting trees, i.e. there is a measureable sampling variance. By constructing a consensus tree, we can

138 partition the data into a variable and a common component. We find that 88% of the branch length is influenced
139 by sampling variance, while the remaining 12% still recover the expected topology (Figure 4C). When we use a read
140 coverage of 1-5 for the same analysis, we find that 52% of the branch length are subject to sampling variance and
141 for all reads combined it is 35% (Figure 4 - figure supplement 3). Hence, at the 100 Mill read level, we have a
142 noticeable effect of sampling variance, but this does not erase the underlying signal. Also, the analysis in Figure 4B
143 is based on 600 Mill reads per taxon, where sampling variance is expected to be further lowered.

144

145 The high dynamics of transcriptional turnover between taxa raises the question whether all parts of the genome
146 might be accessible to transcription at some point in evolutionary time. To explore this possibility, we used a
147 rarefaction approach to simulate the addition of one taxon at a time and used the curve to predict the behavior of
148 adding more taxa than the ones in the present study. We compared this approach to a curve of increasing depth of
149 sequencing, by taking subsets at 10% intervals to understand whether depth or taxonomic diversity have different
150 behavior in this respect. We assume that in each species only a subset of the genome is transcribed, therefore the
151 increase in depth of sequencing would saturate at some point below 100%. Conversely, if each taxon is
152 transcribing slightly different portions of the genome due to a steady turnover, increasing the total number of
153 sampled taxa should increase the saturation more than the increase that could be achieved by sequencing depth.
154 This is indeed what we find. The addition of taxa indeed leads to a further increase in transcriptomic coverage,
155 with a generalized linear model best describing the data as increasing in a logarithmic fashion (Figure 5A). In
156 contrast, we observe an asymptotic behavior of the curve for increasing depth of sequencing, with apparent
157 saturation reached at 84.1%, close to the 83.2% that we have already achieved (Figure 5B).

158

159 Combined with the previous results, this allows two major conclusions. First, random transcriptional noise
160 (technical or biological) or deficiencies in sampling low level transcripts should not be major factors in our analysis,
161 since saturation with sequencing depth would not be possible under a singleton dominated regime. Furthermore,
162 low level transcripts (including singletons) have detectable biological signal (Figure 4C). Second, the data are
163 consistent with the above outlined ideas that the evolutionary turnover leads to steady –and almost unlimited –
164 transcriptional exploration of the genome, when summed over multiple parallel evolutionary lineages and taxa.

165

166 The above overall statistical consideration would still allow for the possibility of the existence of a few scattered
167 genomic islands that are not accessible to transcription because of structural reasons (so-called transcriptional
168 deserts - Montavon and Duboule 2012) or heterochromatically packed because they are not encoding genes
169 required in the respective tissues. Hence, we analyzed also the size distribution of transcript-free genomic regions
170 in our dataset. We find that the maximum observed length of non-transcribed regions is 6kb (Figure 6), suggesting
171 that apparent transcriptional deserts in one taxon are readily accessible to transcription in other taxa, at least for
172 the non-repetitive windows of the genome that are analyzed here.

173
174
175
176
177
178
179
180
181
182
183
184
185
186
187
188
189
190
191
192
193
194
195
196
197
198
199
200
201
202
203
204
205
206
207

Discussion

Various studies have shown that many more regions of the genome are transcribed than are annotated as exons (Ponting and Belgard, 2010; Kapranov and St Laurent, 2012). The significance of this additional transcription has been largely unclear and it has even been considered as noise, either biological or technical. Here we were able to trace the turnover of these extra transcripts. Our data suggest that many have sufficient stability to reflect a phylogenetic distance distribution that mimics the phylogeny of the taxa. Hence, they should not simply be considered as noise. Rather, their lifetime should be sufficient to expose them to evolutionary testing and in this way they become a substrate for *de novo* evolution of genes. On the other hand, they appear to have only a limited lifetime in case they do not acquire a function, i.e. there is also high turnover of the transcribed regions between taxa. This turnover has as a consequence that within a timespan of a few million years practically the whole genome is covered by transcription at some point in time, i.e. no major transcript-free islands exist.

We have here sampled only three tissues. If more tissues and more life stages were sampled, one would expect an even higher coverage of the genome within a given taxon. Such deep analyses have been done in the ENCODE projects (<http://www.genome.gov/10005107>) and they have confirmed pervasive transcription (Clark et al. 2011; Hangauer et al. 2013; Kellis et al. 2014). Still, we expect that the turnover of transcribed regions between taxa would also apply to the other tissues and stages, i.e. evolutionary testing of new transcripts would relate to all tissues and stages. This turnover is contrasted by the set of conserved genes across taxa, for which even the expression levels may be maintained across larger evolutionary distances (Pervouchine et al. 2015).

We see a particularly large number of lineage-specific transcripts among the most closely related taxa. This becomes most evident in the distance tree in Figure 4B where the branch length of the three populations of *M. m. domesticus*, which have separated only a few thousand years ago, are almost as long as those of the sister species *M. spretus* that has separated almost 2 Mill. years ago. Although this is partially influenced by sampling variance of low expressed transcripts (Figure 4C), this suggests that at the very short evolutionary distances (thousands of years) there is an even higher turnover of transcripts than at the longer time frames (millions of years). Such a pattern of unequal rates suggests that weak selection could act against many newly arising transcripts, such that they can exist for a short time at a population scale, but not over an extended time. Hence, we expect that the presence of such transcripts will be polymorphic at the population level, similar as it has been shown in *Drosophila* (Zhao et al. 2014). We have done a preliminary analysis of transcriptional variance between four individuals of each of the taxa and find this expectation fulfilled, but a more extensive study is required to obtain reliable data at this level.

208 We expect that a fraction of new transcripts interacts with other genes and cellular processes, either via providing
209 a positive function or via being slightly deleterious. Our data do not allow at present to speculate on how large this
210 "functional" fraction would be, but this could become subject to future experimental studies. It is also as yet open
211 whether the transcripts exert their functions as RNAs or via translation products. The analysis of ribosome profiling
212 data has shown that many RNAs that were initially classified as non-coding can be associated to ribosomes, i.e. are
213 likely translated (Wilson and Masel 2011; Carvunis et al. 2012; Ruiz-Orera et al. 2014). On the other hand, when
214 tracing the origin of *de novo* genes, one finds frequently that they act first as RNA and acquire open reading frames
215 only at a later stage (Cai et al. 2008; Xie et al. 2012; Reinhardt et al. 2013 - see discussion in Schlötterer 2015). For
216 some of the *de novo* evolved genes in *Drosophila* it has been shown that they have assumed essential functions for
217 the organism, such that knockouts of them are lethal (Chen et al. 2010). Global analyses of new gene emergence
218 trends suggest that the *de novo* evolution process has been active throughout the evolutionary history (Neme and
219 Tautz 2013). Hence, the possibility of a transition from new transcript emergence over acquisition of reading
220 frames towards assuming essential genetic functions is well documented.

221
222 The idea that many *de novo* transcripts are slightly deleterious is concordant with the fact that various cellular
223 processes maintain a balance between RNA transcription and degradation (Houseley & Tollervey, 2009; Jensen et
224 al. 2013). In yeast and mammals it has been shown that several molecular pathways exist that degrade excess
225 transcripts, in particular the ones from bidirectional promoter activity (Jensen et al. 2013; Wu and Sharp 2013).
226 Hence, the fact that many of the transcripts found by deep sequencing occur only at low levels does not
227 necessarily imply a low level of transcription, but could alternatively be due to fast targeting by a degradation
228 machinery.

229
230 Our results provide an evolutionary dynamics perspective where emergence, functionalization and decay of gene
231 functions should be seen as an evolutionary life cycle of genes (Neme and Tautz 2014). *De novo* gene birth should
232 no longer be considered as the result of unlikely circumstances, but rather as an inherent property of the
233 transcriptional apparatus and thus a mechanism for testing and revealing hidden adaptive potential in genomes
234 (Brosius 2005; Masel and Siegal, 2009). Within this evolutionary perspective, any non-genic part of the genome has
235 the possibility to become useful at some time.

236
237

238 **Material and Methods**

239 *Sampled taxa*

240 The youngest divergence point sampled, at about 3,000 years, corresponds to the split between two European
241 populations of *Mus musculus domesticus* (Cucchi et al. 2005) one from France (Massif Central = DOM_{MC}) and one
242 from Germany (Cologne-Bonn area = DOM_{CB}) (Ihle et al. 2006). These European populations in turn have diverged
243 from an ancestral *M. m. domesticus* population in Iran (Ahvaz = DOM_{AH}) about 12,000 years ago (Hardouin et al.
244 2015). The European *M. m. domesticus* are also the closest relatives of the reference genome, the C57BL/6J strain
245 Didiaon and Villena 2013).

246 We included two populations of *Mus musculus musculus*; one from Austria (Vienna = MUS_{VI}) and one from
247 Kazakhstan (Almaty = MUS_{KH}). These two populations are supposed to have a longer divergence between then the
248 European *M. m. domesticus* populations, but a more accurate estimate is currently not available. We set the
249 divergence for analyses at around 10,000 years as an approximate estimate. *M. m. domesticus* has diverged from
250 *M. m. musculus* and *Mus musculus castaneus* about 0.4 to 0.5 million years ago, with a subsequent divergence, not
251 long after, between *M. m. musculus* and *M. m. castaneus* (Suzuki et al. 2013). We included *M. m. castaneus* (CAS)
252 from Taiwan as a representative of the subspecies.

253 To account for longer divergence times, we included *Mus spicilegus* (SPI; estimated divergence of 1.2 million
254 years); *Mus spretus* (SPR; estimated divergence of 1.7 million years) (Suzuki et al. 2013); *Mus mattheyi* (MAT;
255 subgenus *Nannomys*), the North African miniature mouse (estimated divergence of 6.6 million years) (Catzeflis and
256 Denys 1992; Lecompte et al. 2008), and *Apodemus uralensis*, the ural field mouse (APO; estimated divergence of
257 10.6 million years) (Lecompte et al. 2008).

258 The population-level samples (*M. m. domesticus* and *M. m. musculus*) included are maintained under outbreeding
259 schemes, which allows for natural polymorphisms to be present in the samples. All other non-population samples
260 are kept as more or less inbred stock, and therefore fewer polymorphisms are expected. All mice were obtained
261 from the mouse collection at the Max Planck Institute for Evolutionary Biology, following standard rearing
262 techniques which ensure a homogeneous environment for all animals. Mice were maintained and handled in
263 accordance to FELASA guidelines and German animal welfare law (Tierschutzgesetz § 11, permit from Veterinäramt
264 Kreis Plön: 1401-144/PLÖ-004697).

265 A total of 60 mice were sampled, as follows: Eight male individuals from each population-level sample (outbreds),
266 Iran (DOM_{AH}), France (DOM_{MC}), and Germany (DOM_{CB}) of *Mus musculus domesticus*, and Austria (MUS_{VI}) and
267 Kazakhstan (MUS_{KH}) of *Mus musculus musculus*. Four male individuals from the remaining taxa (partially inbred):
268 *Mus musculus castaneus* (CAS), *Mus spretus* (SPR), *Mus spicilegus* (SPI), *Mus mattheyi* (MAT) and *Apodemus*
269 *uralensis* (APO). Mice were sacrificed by CO₂ asphyxiation followed immediately by cervical dislocation. Mice were

270 dissected and tissues were snap-frozen within 5 minutes post-mortem. The tissues collected were liver (ventral
271 view: front right lobe), both testis and whole brain including brain stem.

272 *Genome sequencing*

273 One individual from each of *M. spicilegus*, *M. spretus*, *M. mattheyi*, and *Apodemus uralensis* were selected for
274 genome sequencing. DNA was extracted from liver samples. DNA extraction was performed using a standard salt
275 extraction protocol. Tagged libraries were prepared using the Genomic DNA Sample preparation kit from Illumina,
276 following the manufacturers' instructions. After library preparation, the samples were run in IlluminaHiSeq 2000 at
277 a depth of approximately 2.6 lanes per genome. Library insert size is ~190bases and paired-end reads were 100
278 bases long. Library preparation and sequencing was performed at the Cologne Center for Genomics. Sequencing
279 read statistics are provided in Table 1. Data are available under the study accessions PRJEB11513, PRJEB11533 and
280 PRJEB11535, from the European Nucleotide Archive (<http://www.ebi.ac.uk/ena/>).

281 *Transcriptome sequencing*

282 The sampled tissues of each taxon were used for RNA extraction with the RNAeasy Mini Kit (QIAGEN) and RNA was
283 pooled at equimolar concentrations. RNA quality was measured with the Agilent RNA Nano Kit, for the individual
284 samples and pools. Samples with RIN values above 7.5 were used for sequencing. Library preparation was done
285 using the Illumina TruSeq library preparation, with mRNA purification (poly-A⁺ selection), following manufacturers'
286 instructions. Sequencing was done in Illumina HiSeq 2000 sequencer. Libraries for each group were tagged, pooled
287 and sequenced in a single lane, corresponding to approximately one third of a HiSeq2000 lane. Library insert size is
288 ~190bases and paired-end reads were 100 bases long. Additional sequencing of the brain samples was performed
289 to identify potential limitations in depth of sequencing. For this, each brain library was sequenced on a full lane of
290 a HiSeq2000. All library preparation and sequencing was done at the Cologne Center for Genomics (CCG).
291 Sequencing read statistics are provided in Tables 2 and 3. Data are available under the study accessions
292 PRJEB11513 and PRJEB11533, from the European Nucleotide Archive (<http://www.ebi.ac.uk/ena/>).

293 *Raw data processing*

294 All raw data files were trimmed for adaptors and quality using Trimmomatic (Lohse et al. 2012). The quality
295 trimming was performed basewise, removing bases below quality score of 20 (Q20), and keeping reads whose
296 average quality was of at least Q30. Reads whose trimmed length was shorter than 60 bases were excluded from
297 further analyses, and pairs missing one member because of poor quality were also removed from any further
298 analyses.

299 *Mapping*

300 The reconstruction of transcriptomes using high-throughput sequencing data is not trivial when comparing
301 information across different species to a single reference genome. This is due to the fact that most of the tools

302 designed for such tasks do not work in a phylogenetically aware context. For this reason, any approximation which
303 deals with fractional data (i.e. any high-throughput sequencing setup available to this date) is limited by the
304 detection abilities of the software of choice and by the quality of the reference (transcriptome and genome).

305 Given the high quality state of the mouse genome repositories, we decided to take a reference-based approach, in
306 which all analyses are centered in the reference genome of the C57BL/6 laboratory strain of *Mus musculus*
307 *domesticus*, which enables direct comparisons across all species based on the annotations of the C57BL/6
308 laboratory strain.

309 Transcriptome and genome sequencing reads were aligned against the mm10 version of the mouse reference
310 genome (Waterston et al. 2002) from UCSC (Fujita et al. 2011) using NextGenMap which performs extremely well
311 with divergences of over 10% compared to other standard mapping software (Sedlazeck et al. 2013), as confirmed
312 by our own simulations (Appendix 1). The program was run under default settings, except for --strata 1 and --
313 silent-clip. The first option enforces uniquely mapping reads and the second drops the unmapped portion of the
314 reads, to avoid inflating coverage statistics. This is particularly relevant around exon-intron boundaries, where
315 exonic reads are forced into intronic regions unless this option is set.

316 We produced normalized versions of the alignments per tissue. This was achieved by counting the total amount of
317 uniquely mapped reads in each taxon for each tissue, and sampling without replacement a fraction of each file
318 which would result in the roughly the same absolute number of uniquely mapped reads for all samples of the same
319 tissue (summarized in Table 2).

320

321 *Coverage statistics*

322 We performed coverage statistics on 200 bp windows, to minimize problems derived from the fractional nature of
323 the data, in which a few nucleotides could be absent from a sequenced fragment due to the preparation of the
324 samples, low quality towards read ends, or a few mismatches during mapping. Coverage statistics were computed
325 from normalized alignment files with the featureCounts program from the Subreads suite (Liao et al., 2014). In
326 order to avoid counting reads twice if they would span two windows (which would be the case for most reads), we
327 assigned reads to the window where more than half of the read was present.

328 Genomic reads were used as a metric of empiric mapability for the coverage statistics, i.e. to identify which regions
329 can be reliably detected. For this, we removed from the mapping results against the reference genome (see above)
330 all regions that were not mapped across the phylogeny based on the genomic reads from the taxa more than 1 Mill
331 years apart. The remaining portion we call the 'common genome' in all analyses. It is important to highlight that
332 this is not the same as synteny, since we did not perform any co-linearity analyses between fragments, but rather

333 represent the mere presence in the species, in any possible order. The common genome serves to limit mapping
334 artifacts, since the reads observed in each window must not only be uniquely mapping, but also be present and
335 detectable in all the genomes considered.

336 We report coverage only from windows in the common genome for several reasons. First, we want to compare
337 changes in transcription in regions which are present across all taxa, so the region must be present at the genome
338 level. Second, the observation of transcriptome coverage on a region of the reference genome without genomic
339 coverage from the respective taxon could represent mapping artifacts. Thus by enforcing coverage on both levels,
340 and in all taxa at the genomic level, we reduce mapping artifacts and errors. Third, we assume that the
341 transcriptional properties of the common genome should be general enough that they represent the properties of
342 each of the genomes of the taxa under study. Summary data for coverage of all genomes and transcriptomes are
343 available under the Dryad accession associated with this manuscript (doi:10.5061/dryad.8jb83)

344 *Reconstruction of phylogenetic relationships*

345 We performed genome-wide correlations of coverage to infer distance between the taxa under study. Correlations
346 of two types were initially used: rank-based (spearman correlation) and binary (phi correlation). From correlation
347 matrices, we constructed manhattan distance matrices and from those we further constructed neighbor-joining
348 trees to describe the proximity between any two taxa based on shared transcriptome information. We focus
349 mostly on the presence or absence of transcriptional coverage. For this reason, we used only the binary
350 correlations in the figures. In this representation, closely related organisms have more shared transcriptomic
351 coverage than distantly related organisms. Analyses were performed in R, using the function `dist()` from the `stats`
352 package and `nj()` from the `ape` package (Paradis et al. 2004).

353 Additionally, whole mitochondrial genomes were obtained for each taxon as consensus sequences from mapped
354 reads using `samtools mpileup` (Li et al. 2009). The sequences were aligned with `MUSCLE` (Edgar 2004), and a NJ
355 tree was constructed with the `dist.dna()` and `nj()` functions from the `ape` package (Paradis et al. 2004). All trees
356 were tested with 1000 bootstraps with the `boot.phylo()` function from the `ape` package. Reported nodes have a
357 support of 70% or greater.

358

359 *Estimation of sampling variance from brain samples*

360 The extensive sequencing of brain samples were used to obtain estimates of how sampling might affect the
361 terminal branch lengths of trees based on low coverage regions. For this, we split the alignments into three non-
362 overlapping sets of 100 million reads per taxon, such that each set would contain sets of independent
363 observations. Paired-read relationships were maintained, so that pairs of the same fragments would be in the
364 same set. From this, we obtained trees as mentioned before, and the portions of the branches of each taxon which

365 were shared across sets were considered as robust to sampling biases, while the discordant portions between
366 samples were considered to be due to sampling variance. Summary data from subsampled sets are available under
367 the Dryad accession associated with this manuscript (doi:10.5061/dryad.8jb83).

368 *Rarefaction and subsampling*

369 Transcriptome experiments tend to be limited by the depth of sequencing, with highly expressed genes being
370 relatively easy to sample, and rare transcripts becoming increasingly difficult to find. Given the large amount of
371 data generated, we investigated whether our data show signals of coverage saturation from subsets of the data of
372 different sizes. The total experiment, comprising ten taxa, corresponds to 6.4×10^9 reads (or 6.4 billion reads). We
373 subsampled (samtools view -s) portions of mapped reads for each taxon, ranging between 10% to 100%, at 10%
374 intervals. The observation of coverage saturation in this case would indicate that our sequencing efforts likely
375 cover most of the transcribed regions of the common genome. Summary data are available under the Dryad
376 accession associated with this manuscript (doi:10.5061/dryad.8jb83).

377 In parallel, we estimated the individual and combined contribution of each taxon to the transcriptomic coverage of
378 the common genome. Not all samples have the same phylogenetic distance to each other (some species have
379 more representatives than others). To account for this we generated one hundred arrays of the ten taxa with
380 random order, and recorded the coverage after the addition of each taxon in each array. The observation of
381 coverage saturation in this setup would indicate that taxonomic sampling is sufficient to cover most of the
382 potentially transcribed regions of the common genome.

383 In order to estimate whether our data continued to increase or approached saturation, we tested two alternative
384 models: a generalized linear model with logarithmic behavior (ever increasing) or a self-starting nonlinear
385 regression model (saturating). The best fit was decided based on the minimum BIC value between the two models,
386 and an estimate of the Bayes factor was computed from the difference of BIC values and support was obtained
387 from standard criteria (Kass and Raftery, 1995). Analyses were performed in R, using the functions glm(), nls(),
388 SSasymp(), and BIC() from the stats package (R Core Team, 2014).

389 *Analysis of transcribed and non-transcribed regions across the genome*

390 Transcribed and non-transcribed windows of the common genome were defined by the continuous presence or
391 absence of transcriptomic coverage from mapping information of each taxon and tissue. Neighboring transcribed
392 regions across species were combined to obtain stretches of transcriptionally active common genome.

393 *Enrichment of annotations from the mouse reference*

394 Annotations of *Mus musculus* from Ensembl v81 (Cunningham et al, 2015) were used to infer the relative
395 contribution of known genes to the observed transcription across species. We partitioned the sets between genes,
396 exons, and introns, and those were further partitioned between protein-coding and non-coding genes. To

397 determine if the overlaps are significantly different from a random distribution of the features along the genome,
398 we randomized 1000 times each of the annotated intervals (genes, exons, introns, and subsets of coding and non-
399 coding) along the genome using shuffleBed from the bedtools suite (Quinlan & Hall, 2010), and compared the
400 overlap to various transcribed regions (single taxa, less than 9 taxa, more than 8 taxa, 10 taxa, and transcribed in
401 any taxon). Multiple testing corrections were performed and significant comparisons are reported at 5% FDR.
402 Furthermore, since we assume that most annotations fall within transcribed regions in any species, we used the
403 total transcriptomic coverage across all taxa to calculate potential discrepancies in the shuffling method. The ratios
404 of expected and observed coverage of total transcription across taxa for a given feature were calculated to define
405 the range of ratios for which comparisons were also non-significant, i.e., where we could not rule out method bias.

406

407 **Acknowledgements**

408 We thank the C. Pfeifle and the mouse team for providing the animals, N. Thomsen for technical assistance, J.
409 Altmüller and C. Becker for sequencing, B. Harr, A. Nolte, C. Xie, L. Pallares and L. Turner for comments on the
410 manuscript and the members of our group for discussions and suggestions. Special thanks to F. Sedlazeck for
411 bioinformatic advice and provision of software before publication. R.N. was supported by a PhD fellowship of the
412 IMPRS for Evolutionary Biology during the initial phase of the project. The project was financed through an ERC
413 advanced grant to D.T. (NewGenes - 322564).

414

415 **Author contribution**

416 DT and RN conceived the project, RN did the experimental work and data analysis, DT and RN discussed the data
417 interpretation and wrote the manuscript.

418

419

420

421 **References**

- 422 Brosius, J. 2005. Waste not, want not—transcript excess in multicellular eukaryotes. *Trends Genet.* **21**: 287–288.
- 423 Cai J, Zhao RP, Jiang HF, Wang W (2008) De novo origination of a new protein-coding gene in *Saccharomyces*
424 *cerevisiae*. *Genetics* **179**, 487-496.
- 425 Carvunis AR, Rolland T, Wapinski I, *et al.* (2012) Proto-genes and de novo gene birth. *Nature* **487**, 370-374.
- 426 Catzefflis FM, Denys C (1992) The african *Nannomys* (Muridae) - an early offshoot from the *Mus* lineage - evidence
427 from scDNA hybridization experiments and compared morphology. *Israel Journal of Zoology* **38**, 219-231.
- 428 Chen SD, Zhang YE, Long MY (2010) New Genes in *Drosophila* Quickly Become Essential. *Science* **330**, 1682-1685.
- 429 Clark MB, Amaral PP, Schlesinger FJ, *et al.* (2011) The Reality of Pervasive Transcription. *Plos Biology* **9**.
- 430 Cucchi T, Vigne JD, Auffray JC (2005) First occurrence of the house mouse (*Mus musculus domesticus* Schwarz &
431 Schwarz, 1943) in the Western Mediterranean: a zooarchaeological revision of subfossil occurrences.
432 *Biological Journal of the Linnean Society* **84**, 429-445.
- 433 Cunningham F, Amode MR, Barrell D, *et al.* (2015) Ensembl 2015. *Nucleic Acids Research* **43**, D662-D669.
- 434 Didion JP, de Villena FP-M (2013) Deconstructing *Mus gemischus*: advances in understanding ancestry, structure,
435 and variation in the genome of the laboratory mouse. *Mammalian Genome* **24**, 1-20.
- 436 Edgar RC (2004) MUSCLE: multiple sequence alignment with high accuracy and high throughput. *Nucleic Acids*
437 *Research* **32**, 1792-1797.
- 438 Gotea V, Petrykowska HM, Elnitski L (2013) Bidirectional Promoters as Important Drivers for the Emergence of
439 Species-Specific Transcripts. *Plos One* **8**.
- 440 Hangauer MJ, Vaughn IW, McManus MT (2013) Pervasive Transcription of the Human Genome Produces
441 Thousands of Previously Unidentified Long Intergenic Noncoding RNAs. *Plos Genetics* **9**, 13.
- 442 Heinen T, Staubach F, Haming D, Tautz D (2009) Emergence of a New Gene from an Intergenic Region. *Current*
443 *Biology* **19**, 1527-1531.
- 444 Houseley J, Tollervey D (2009) The Many Pathways of RNA Degradation. *Cell* **136**, 763-776.
- 445 Ihle S, Ravaoarimanana I, Thomas M, Tautz D (2006) An analysis of signatures of selective sweeps in natural
446 populations of the house mouse. *Molecular Biology and Evolution* **23**, 790-797.
- 447 Jensen TH, Jacquier A, Libri D (2013) Dealing with Pervasive Transcription. *Molecular Cell* **52**, 473-484.
- 448 Kapranov P1, St Laurent G (2012). Dark Matter RNA: Existence, Function, and Controversy. *Front Genet.* 3:60. doi:
449 10.3389/fgene.2012.00060.
- 450 Kapusta A, Feschotte C (2014) Volatile evolution of long noncoding RNA repertoires: mechanisms and biological
451 implications. *Trends in Genetics* **30**, 439-452.
- 452 Kass R, Raftery A (1995) Bayes Factors. *Journal of the American Statistical Association* **90**, 430:773-795.
- 453 Karolchik D, Barber GP, Casper J, *et al.* (2014) The UCSC Genome Browser database: 2014 update. *Nucleic Acids*
454 *Research* **42**, D764-D770.
- 455 Keane TM, Goodstadt L, Danecek P, *et al.* (2011) Mouse genomic variation and its effect on phenotypes and gene

456 regulation. *Nature* **477**, 289-294.

457 Kellis M, Wold B, Snyder MP, *et al.* (2014) Defining functional DNA elements in the human genome. *Proceedings of*
458 *the National Academy of Sciences of the United States of America* **111**, 6131-6138.

459 Knowles DG, McLysaght A (2009) Recent de novo origin of human protein-coding genes. *Genome Research* **19**,
460 1752-1759.

461 Kutter C, Watt S, Stefflova K, *et al.* (2012) Rapid Turnover of Long Noncoding RNAs and the Evolution of Gene
462 Expression. *Plos Genetics* **8**.

463 Lecompte E, Aplin K, Denys C, *et al.* (2008) Phylogeny and biogeography of African Murinae based on
464 mitochondrial and nuclear gene sequences, with a new tribal classification of the subfamily. *Bmc*
465 *Evolutionary Biology* **8**.

466 Li H, Handsaker B, Wysoker A, *et al.* (2009) The Sequence Alignment/Map format and SAMtools. *Bioinformatics* **25**,
467 2078-2079.

468 Liao Y, Smyth GK, Shi W (2014) featureCounts: an efficient general-purpose program for assigning sequence reads
469 to genomic features. *Bioinformatics* **30**(7):923-30.

470 Lohse M, Bolger AM, Nagel A, *et al.* (2012) RobiNA: a user-friendly, integrated software solution for RNA-Seq-based
471 transcriptomics. *Nucleic Acids Research* **40**, W622-W627.

472 Masel J, Siegal ML (2009) Robustness: mechanisms and consequences. *Trends in Genetics* **25**, 395-403.

473 Montavon T, Duboule D (2012) Landscapes and archipelagos: spatial organization of gene regulation in
474 vertebrates. *Trends in Cell Biology* **22**, 347-354.

475 Necsulea A, Kaessmann H (2014) Evolutionary dynamics of coding and non-coding transcriptomes. *Nature Reviews*
476 *Genetics* **15**, 734-748.

477 Neme R, Tautz D (2013) Phylogenetic patterns of emergence of new genes support a model of frequent de novo
478 evolution. *Bmc Genomics* **14**.

479 Neme R, Tautz D (2014) Evolution: Dynamics of De Novo Gene Emergence. *Current Biology* **24**, R238-R240.

480 Palmieri N, Kosiol C, Schlötterer C (2014) The life cycle of Drosophila orphan genes. *Elife* **3**.

481 Paradis E, Claude J, Strimmer K (2004) APE: Analyses of Phylogenetics and Evolution in R language. *Bioinformatics*
482 **20**, 289-290.

483 Pervouchine DD, Djebali S, Breschi A, Davis CA, Barja PP, Dobin A, Tanzer A, Lagarde J, Zaleski C, See LH, Fastuca M,
484 Drenkow J, Wang H, Bussotti G, Pei B, Balasubramanian S, Monlong J, Harmanci A, Gerstein M, Beer MA9,
485 Notredame C, Guigó R, Gingeras TR (2025). Enhanced transcriptome maps from multiple mouse tissues
486 reveal evolutionary constraint in gene expression. *Nat Commun.* 6:5903. doi: 10.1038/ncomms6903.

487 Ponting CP, Belgard TG (2010). Transcribed dark matter: meaning or myth? *Hum Mol Genet.* 19:R162-168. doi:
488 10.1093/hmg/ddq362.

489 Quinlan AR, Hall IM (2010) BEDTools: a flexible suite of utilities for comparing genomic features. *Bioinformatics* **26**,
490 841-842.

491 R Core Team. *R: A language and environment for statistical computing*. (R Foundation for Statistical Computing,
492 Vienna, Austria, 2014). at <<http://www.R-project.org/>>

493 Reinhardt JA, Wanjiru BM, Brant AT, *et al.* (2013) De Novo ORFs in Drosophila Are Important to Organismal Fitness
494 and Evolved Rapidly from Previously Non-coding Sequences. *Plos Genetics* **9**.

495 Ruiz-Orera J, Messeguer X, Subirana JA, Alba MM (2014) Long non-coding RNAs as a source of new peptides. *Elife*

496 Ruiz-Orera J, Hernandez-Rodriguez J, Chiva C, Sabidó E, Kondova I, Bontrop R, Marqués-Bonet T, Albà MM (2015)
497 Origins of De Novo Genes in Human and Chimpanzee. *PLoS Genet.* 2015 Dec 31;11(12):e1005721. doi:
498 10.1371/journal.pgen.1005721

499 Schlötterer C (2015). Genes from scratch-the evolutionary fate of de novo genes. *Trends Genet* 31:215-219. doi:
500 10.1016/j.tig.2015.02.007

501 Sedlazeck FJ, Rescheneder P, von Haeseler A (2013) NextGenMap: fast and accurate read mapping in highly
502 polymorphic genomes. *Bioinformatics* **29**, 2790-2791.

503 Sundaram V, Cheng Y, Ma ZH, *et al.* (2014) Widespread contribution of transposable elements to the innovation of
504 gene regulatory networks. *Genome Research* **24**, 1963-1976.

505 Suzuki H, Nunome M, Kinoshita G, *et al.* (2013) Evolutionary and dispersal history of Eurasian house mice *Mus*
506 *musculus* clarified by more extensive geographic sampling of mitochondrial DNA. *Heredity* **111**, 375-390.

507 Tautz D, Domazet-Lošo T (2011) The evolutionary origin of orphan genes. *Nature Reviews Genetics* **12**, 692-702.

508 Tautz D, Neme R, Domazet-Lošo T (2013) Evolutionary Origin of Orphan Genes. In: eLS. John Wiley & Sons, Ltd:
509 Chichester. DOI: 10.1002/9780470015902.a0024601

510 Waterston RH, Lindblad-Toh K, Birney E, *et al.* (2002) Initial sequencing and comparative analysis of the mouse
511 genome. *Nature* **420**, 520-562.

512 Wu XB, Sharp PA (2013) Divergent Transcription: A Driving Force for New Gene Origination? *Cell* **155**, 990-996.

513 Xie C, Zhang YE, Chen JY, *et al.* (2012) Hominoid-Specific De Novo Protein-Coding Genes Originating from Long
514 Non-Coding RNAs. *Plos Genetics* **8**.

515 Zhao L, Saelao P, Jones CD, Begun DJ (2014) Origin and Spread of de Novo Genes in *Drosophila melanogaster*
516 Populations. *Science* **343**, 769-772.

517

518 **Tables**519 Table 1. Genome sequencing and read mapping information relative to the C57Bl/6 reference strain
520 (GRCm38.3/mm10).

Species	Uniquely mapping reads (MAPQ >25)	Mean coverage depth (window based)	Reference coverage (% windows)	Total sequence divergence*	Accession Reads	Accession BAMs
<i>Apodemus uralensis</i>	4.46E+08	40x	78.23%	5.60%	ERS942341	ERS946059
<i>Mus mattheyi</i>	5.58E+08	52x	77.19%	4.50%	ERS942343	ERS946060
<i>Mus spretus</i>	7.71E+08	52x	93.91%	1.70%		ERS946096**
<i>Mus spicilegus</i>	6.16E+08	57x	84.39%	1.60%	ERS942342	ERS946061

521 * The percentage of divergence was estimated from mappings using NextGenMap (Sedlazeck et al.
522 2013). Only uniquely mapping reads were considered and mapping quality greater than 25. Variation
523 was estimated from the alignments using samtools mpileup (Li et al. 2009). Divergence was calculated as
524 number of changes divided by the genome size.

525 ** Corresponds to study accession PRJEB11535. All other accessions deposited under studies
526 PRJEB11513 and PRJEB11533.

527

528 Table 2. Transcriptome reads from each sample sequenced, mapped and normalized.

Taxon Code	Tissue	Lanes	QC-passed reads	Mapped reads	(% total)	Normalized subset	(%total)	(% mapped)	Accession Reads*	Accession BAMs**
DOMCB	Brain	0.33x	1.30E+08	1.26E+08	96%	9.15E+07	70%	73%	ERS946023	ERS942305
DOMCB	Liver	0.33x	1.41E+08	1.17E+08	83%	9.07E+07	64%	77%	ERS946025	ERS942306
DOMCB	Testis	0.33x	1.26E+08	1.22E+08	96%	1.19E+08	94%	98%	ERS946026	ERS942307
DOMMC	Brain	0.33x	1.17E+08	1.13E+08	96%	9.15E+07	78%	81%	ERS946027	ERS942309
DOMMC	Liver	0.33x	1.34E+08	1.09E+08	81%	9.07E+07	68%	84%	ERS946029	ERS942310
DOMMC	Testis	0.33x	1.42E+08	1.37E+08	96%	1.19E+08	83%	87%	ERS946030	ERS942311
DOMAH	Brain	0.33x	9.49E+07	9.15E+07	96%	9.15E+07	96%	100%	ERS946019	ERS942301
DOMAH	Liver	0.33x	1.16E+08	1.02E+08	88%	9.07E+07	78%	89%	ERS946021	ERS942302
DOMAH	Testis	0.33x	1.61E+08	1.55E+08	96%	1.19E+08	74%	77%	ERS946022	ERS942303
MUSKH	Brain	0.33x	1.33E+08	1.28E+08	96%	9.15E+07	69%	72%	ERS946035	ERS942313
MUSKH	Liver	0.33x	1.03E+08	9.07E+07	88%	9.07E+07	88%	100%	ERS946037	ERS942314
MUSKH	Testis	0.33x	1.36E+08	1.31E+08	96%	1.19E+08	87%	91%	ERS946038	ERS942315
MUSVI	Brain	0.33x	1.23E+08	1.19E+08	96%	9.15E+07	74%	77%	ERS946031	ERS942317
MUSVI	Liver	0.33x	1.23E+08	9.47E+07	77%	9.07E+07	74%	96%	ERS946033	ERS942318
MUSVI	Testis	0.33x	1.32E+08	1.27E+08	96%	1.19E+08	90%	93%	ERS946034	ERS942319
CAS	Brain	0.33x	1.21E+08	1.16E+08	96%	9.15E+07	76%	79%	ERS946039	ERS942321
CAS	Liver	0.33x	1.23E+08	1.01E+08	82%	9.07E+07	74%	90%	ERS946041	ERS942322
CAS	Testis	0.33x	1.23E+08	1.19E+08	96%	1.19E+08	96%	100%	ERS946042	ERS942323

SPI	Brain	0.33x	1.34E+08	1.29E+08	96%	9.15E+07	68%	71%	ERS946043	ERS942325
SPI	Liver	0.33x	1.05E+08	9.82E+07	93%	9.07E+07	86%	92%	ERS946045	ERS942326
SPI	Testis	0.33x	1.44E+08	1.38E+08	96%	1.19E+08	83%	86%	ERS946046	ERS942327
SPR	Brain	0.33x	1.09E+08	1.05E+08	96%	9.15E+07	84%	87%	ERS946047	ERS942329
SPR	Liver	0.33x	1.35E+08	1.20E+08	89%	9.07E+07	67%	76%	ERS946049	ERS942330
SPR	Testis	0.33x	1.34E+08	1.29E+08	96%	1.19E+08	88%	92%	ERS946050	ERS942331
MAT	Brain	0.33x	1.12E+08	1.04E+08	93%	9.15E+07	82%	88%	ERS946051	ERS942333
MAT	Liver	0.33x	1.23E+08	1.12E+08	91%	9.07E+07	74%	81%	ERS946053	ERS942334
MAT	Testis	0.33x	1.32E+08	1.23E+08	93%	1.19E+08	90%	97%	ERS946054	ERS942335
APO	Brain	0.33x	1.36E+08	1.18E+08	87%	9.15E+07	67%	78%	ERS946055	ERS942337
APO	Liver	0.33x	1.13E+08	1.00E+08	89%	9.07E+07	80%	91%	ERS946057	ERS942338
APO	Testis	0.33x	1.38E+08	1.20E+08	87%	1.19E+08	86%	99%	ERS946058	ERS942339

529 All accessions deposited under studies PRJEB11533* and PRJEB11513**.

530

531

532 Table 3. Additional sequencing effort, focused only on brain samples. Reads sequenced, mapped and
533 normalized.

Taxon Code	Tissue	Lanes	QC-passed reads	Mapped reads	(% total)	Normalized subset	(% total)	(% mapped)	Accession Reads	Accession BAMs
DOMCB	Brain	1x	3.89E+08	3.76E+08	97%	3.19E+08	82%	85%	ERS946024	ERS942308
DOMMC	Brain	1x	3.76E+08	3.64E+08	97%	3.19E+08	85%	88%	ERS946028	ERS942312
DOMAH	Brain	1x	3.46E+08	3.35E+08	97%	3.19E+08	92%	95%	ERS946020	ERS942304
MUSKH	Brain	1x	4.64E+08	4.49E+08	97%	3.19E+08	69%	71%	ERS946036	ERS942316
MUSVI	Brain	1x	4.13E+08	4.00E+08	97%	3.19E+08	77%	80%	ERS946032	ERS942320
CAS	Brain	1x	4.35E+08	4.21E+08	97%	3.19E+08	73%	76%	ERS946040	ERS942324
SPI	Brain	1x	4.31E+08	4.16E+08	97%	3.19E+08	74%	77%	ERS946044	ERS942328
SPR	Brain	1x	3.87E+08	3.73E+08	96%	3.19E+08	82%	85%	ERS946048	ERS942332
MAT	Brain	1x	3.62E+08	3.40E+08	94%	3.19E+08	88%	94%	ERS946052	ERS942336
APO	Brain	1x	4.33E+08	3.77E+08	87%	3.19E+08	74%	84%	ERS946056	ERS942340

534 All accessions deposited under studies PRJEB11533* and PRJEB11513**.

535

536

537
538
539
540
541
542
543
544

545
546
547
548
549
550
551
552
553
554

555
556
557
558
559
560
561
562
563

564
565
566
567
568
569
570
571
572
573
574
575

Figure legends

Figure 1: Phylogenetic relationships and time estimates for the taxa used in the study. New genome sequences were generated for taxa with *. A common genome was constructed across all taxa (Figure 1–figure supplement 1) based on a mapping algorithm that is not affected by the sequence divergence between the samples (Appendix 1). Figure 1–figure supplement 2 shows the intersection of genome coverage between the named species.

Figure 2: Transcriptome coverage of the common genome per taxon. A-C. Liver, brain and testis, respectively, sequenced at approximately the same depth. D. Combination of samples from A-D. E. Additional sequencing of brain samples at 3x depth, compared to B. F. Combination of all samples, including additional brain sequencing. Three coverage levels are represented by colors from light blue to dark blue: window coverage with at least 1, 10 and 100 reads. Taxon abbreviations as summarized in Figure 1, with closest to the reference genome to the left of each panel and most divergent one to the right. Note that the slight rise in low read coverage for the distant taxa could partially be due to slightly more mismapping of reads at this phylogenetic distance (see Appendix 1 for simulation of mapping efficiency), but is also affected by a larger fraction of singleton reads (compare Figure 4-figure supplement 1).

Figure 3: Distribution of shared and non-shared windows with transcripts for each taxon, based on the aggregate dataset across all three tissues. Three classes are represented: i) windows that are found in a single taxon only, ii) windows found in 2-9 taxa and iii) windows shared among all 10 taxa (from left to right in each panel). Windows with transcripts were first classified as belonging to one of the three classes, independent of their coverage, and were then assigned to the coverage classes represented by the blue shading (from light blue to dark blue: window coverage with at least 1, 10 and 100 reads). Taxon names as summarized in Figure 1. Figure 3–figure supplement 1 shows an extended version where class ii) is separated into each individual group. Relative enrichment of annotated genes in the conserved class is shown in Figure 3-figure supplement 2.

Figure 4: Distance tree comparisons based on molecular and transcriptome sharing data. (A) molecular phylogeny based on whole mitochondrial genome sequences as a measure of molecular divergence (black lines represent the branch lengths, dashed lines serve to highlight short branches). (B) tree based on shared transcriptome coverage of the genome, using correlations of presence and absence of transcription of the common genome. All nodes have bootstrap support values of 70% or more (n= 1,000). (C) tree based on shared transcriptome coverage of singleton reads only from subsampling of the extended brain transcriptomes. Left is the consensus tree with the variance component between samples depicted as triangles, right is the same tree, but only for the branch fraction that is robust to sampling variance. Taxon names as summarized in Figure 1. Figure 4–figure supplement 1 shows the fraction of singletons in dependence of each sample in each taxon, Figure 4–figure supplement 2 in dependence of read depth. Figure 4–figure supplement 3 shows an extended version of the analysis shown in 4C for higher coverage levels.

Figure 5: Rarefaction, subsampling and saturation patterns using all available samples and reads. A. Sequencing depth saturation as estimated from an increase in the number of taxa. B. Sequencing depth saturation as estimated from increasing read number. Blue dots indicate increases per sub-sampled sequence fraction or taxon added from our dataset. Gray dotted line indicates the predicted behavior from the indicated regression, and gray

580 area shows the prediction after doubling the current sampling either by additional taxa (A) or in sequencing effort
581 (B). Each analysis was tested for logarithmic and asymptotic models. Best fit was selected from Δ BIC, with Bayes
582 factor shown and qualitative degree of support shown. Standard deviations are shown as black lines in A, and are
583 too small to display in B (note that due to the sampling scheme for this analysis, the values above 50% are not
584 statistically independent and that the 100% value constitutes a single data point without variance measure).

585
586 **Figure 6:** Comparative analysis of lengths of regions transcribed or not transcribed across all data (including deeper
587 brain sequencing) in all samples. Size distribution of regions not covered in any transcript (green) versus size
588 distribution of regions with at least one transcript (blue).

589
590

591 **Legends for supplementary Figures and Files**

592 **Figure 1–figure supplement 1:** Scheme for the establishment of the "common genome" using genomic reads and
593 the mouse reference genome. The common genome represents the portion of the reference which is present and
594 detectable across all species. The genome sequencing, processing and sequence analysis were done in the same
595 way as for transcriptomes, effectively removing possible biases derived from sequencing and mapping. Note that
596 the assignment of the common genome fraction was done after mapping all genomic and transcriptomic reads to
597 the reference, i.e. the mapping process was not affected by a reduced mapping target.

598 **Figure 1–figure supplement 2:** Venn diagrams of representation of the common genome, derived from 200bp
599 windows covered in genomic reads in species with more than one million years divergence to the reference.
600 Windows covered by all four species is used as the common genome (shown as the intersection of all species).

601 **Figure 3–figure supplement 1:** Distribution of shared transcripts according to the number of taxa shared, based on
602 the aggregate dataset across all three tissues. Windows with transcripts were first classified as belonging to each
603 of the sharing categories (from 1 to 10), independent of their coverage, and were then assigned to the coverage
604 classes represented by the blue shading (from light blue to dark blue: window coverage with at least 1, 10 and 100
605 transcripts). Taxon names as summarized in Figure 1.

606 **Figure 3–figure supplement 2.** Windows transcribed across most species (9 or more) are strongly enriched in
607 genes known from the reference genome, while windows transcribed in some taxa (8 or less) are strongly depleted
608 from known genes. The effect is most evident for protein-coding genes, but still present for non-coding genes.

609 **Figure 4–figure supplement 1:** Fraction of windows with singletons (one paired read) of the common genome per
610 taxon. A-C. Liver, brain and testis, respectively, sequenced at approximately the same depth. D. Combination of
611 samples from A-D. E. Additional sequencing of brain samples at 3x depth, compared to B. F. Combination of all
612 samples, including additional brain sequencing. Light gray indicates singletons observed in each individual
613 sample/taxon combination. Dark gray indicates singletons across the whole experiment, i.e. not re-detected in any
614 other tissue or taxon. Taxon abbreviations as summarized in Figure 1, with closest to the reference genome to the
615 left of each panel and most divergent one to the right. Note that the rise in singleton number for the distant taxa
616 can be ascribed to the longer branch length, i.e. absence of closely related taxa in which the singleton could have
617 been re-detected.

618 **Figure 4–figure supplement 2:** Reduction of singletons in dependence of aggregate sequencing depth.

619 **Figure 4–figure supplement 3:** Trees based on shared transcriptome coverage of the genome, using binary
620 correlations. We used the deep sequenced brain samples to estimate the proportion of sampling artifacts in

621 terminal branches, and effectively subtracted the proportion of artifacts to obtain reliable phylogenetic signals.
622 Each brain sample was split in three completely independent samples of 100 million reads. Top: Trees constructed
623 using: regions covered only with one read in each taxon, regions covered by 1 and 5 reads (very low expression),
624 regions covered by any reads, regions above 10 reads (mid expression) and regions above 100 reads (high
625 expression). The percentage shown indicates the average level of sampling artifacts for each threshold, derived
626 from the length of the terminal branches not found in all replicates of each taxon, i.e. the uncorrelated portion
627 across samples of the same origin. These numbers are greatest for the lowest expressed regions, and are lowest
628 for the highly expressed regions, and are more or less constant within comparisons. Once subtracted, the
629 phylogenetic signal remains robust. Taxon names as summarized in Figure 1. The figure part with the 1 read
630 fraction corresponds to Figure 4C.

631

632 **Appendix 1**

633

634 Simulation of mapping efficiency depending on sequence variation

635 We performed simulations of the mapping efficiency of two mappers NextGenMap (NGM) and Bowtie2
636 (standard mapper) across a range of divergences based on the chromosome 19 of the mouse reference
637 genome (mm10 from UCSC). Mutated versions of chromosome 19 were generated with a python script
638 by choosing to randomly substitute a given fraction of the nucleotides in the sequence in random
639 positions along the genome. From each mutated version we simulated sequencing reads with ART
640 (Huang et al. 2012), with a mean fold coverage of 5x (1x standard deviation) and using the same
641 conditions as in our main sequencing experiment (100 bp paired end reads, 190bp fragments) and the
642 options for empirical read quality of the Illumina HiSeq2000 sequencer.

643 Reads were subsequently mapped to the chromosome 19 reference sequence with NextGenMap using
644 the default parameters except for --strata 1 --silent-clip to obtain uniquely mapping reads and to
645 remove the non-mapping regions from reads. Reads were also mapped with Bowtie2, following default
646 parameters except for --very-sensitive. Information about uniquely mapping reads from NGM was
647 derived directly from the bam files and from Bowtie2 was derived from the standard error log files.
648 From Table 1 and Figure 1, we observe that NextGenMap performs extremely well with increasing
649 divergences, and greatly outperforms the standard mapper. While the average difference between the
650 most distant genomes analyzed is about 6%, it must be noted that fast evolving regions of the genome
651 can quickly exceed the mean. NextGenMap is able to capture most of the regions of the genome to
652 allow comparisons across very divergent taxa.

653 In addition to this, we used the set of reads simulated from the chromosome 19 reference sequence and
654 mapped them with NextGenMap to each mutated version of the reference chromosome 19 using the
655 same parameters mentioned above (Figure2; Tables 2 and 3). This allowed the control of accuracy in
656 read placement across divergent sequences by testing the position of each read in each mapping
657 exercise (Figure 2a; Table 2). This was done with the bedtools suite, intersecting reads from each
658 divergent genome to the original, and counting the reads which were in the same location. Reads were

659 allowed to be offset by 20% (80% overlap), for example in in cases where ends would not map
660 successfully. From this we also derived comparable statistics for total uniquely mapped reads, proper
661 paired reads, paired reads regardless of location and single reads mapped where the pair failed to map
662 (Figure 2b; Table 3).

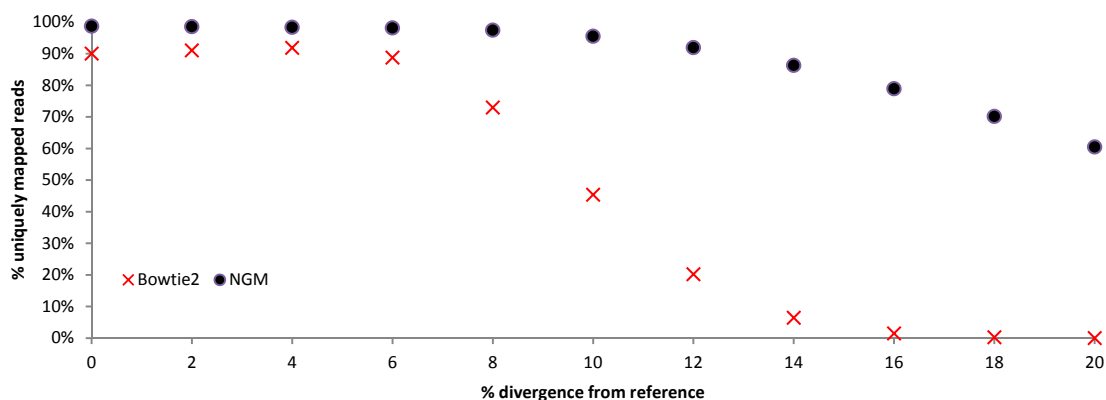
663

664

665 Appendix1 - Table 1. Simulations comparing bowtie2 to NextGenMap. Divergent reads were mapped to
666 a common reference.

total simulated reads	%simulated divergence (reads)	Uniquely mapped reads Bowtie2	Uniquely mapped reads NGM	Percentage unique from total reads Bowtie2	Percentage unique from total reads NGM
2910370	0%	2621200	2873481	90.1%	98.7%
2910982	2%	2650274	2868279	91.0%	98.5%
2911312	4%	2674738	2863581	91.9%	98.4%
2910286	6%	2583320	2856060	88.8%	98.1%
2910978	8%	2124958	2836119	73.0%	97.4%
2910446	10%	1321494	2779837	45.4%	95.5%
2910610	12%	587862	2675011	20.2%	91.9%
2910196	14%	186828	2510840	6.4%	86.3%
2910090	16%	42986	2296917	1.5%	78.9%
2909992	18%	7488	2041437	0.3%	70.2%
2910022	20%	936	1759924	0.0%	60.5%

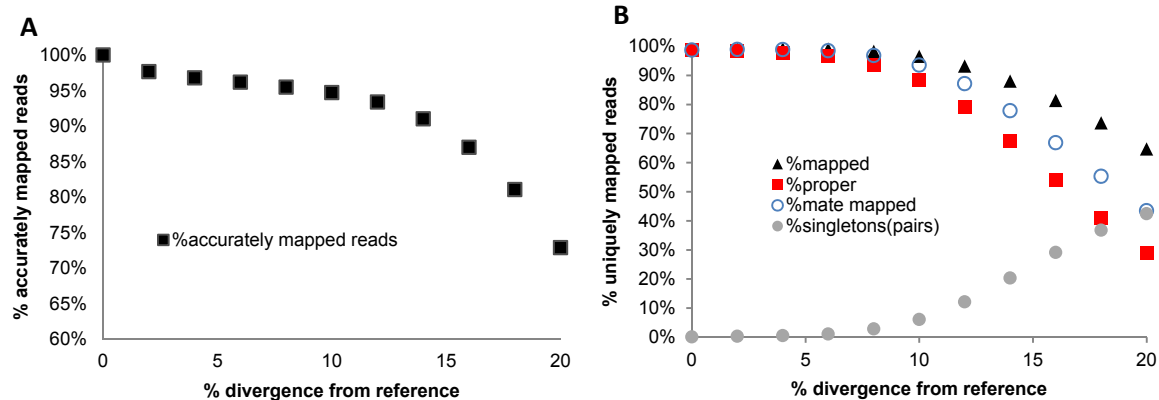
667



668

669 Appendix1 - Figure 1. Performance of NextGenMap compared to Bowtie2.

670



671

672 Appendix1 - Figure 2. Performance of NextGenMap in terms accuracy of mapping using the same set of
 673 reads and increasingly divergent versions of the reference genome (A), and paired-end mapping
 674 statistics (B).

675 Appendix1 - Table 2. Accuracy of NextGenMap. The same set of reads was mapped to divergent genome
 676 versions of the reference. We are assuming that the reads coming from the same reference are correctly
 677 mapped, and used that as a standard for the divergent genomes, so the estimates should be slightly
 678 inflated.

%divergence	accurately mapped reads	%
0%	2910370	100.0%
2%	2842076	97.7%
4%	2816628	96.8%
6%	2798936	96.2%
8%	2778608	95.5%
10%	2756194	94.7%
12%	2717420	93.4%
14%	2648472	91.0%
16%	2531728	87.0%
18%	2358964	81.1%
20%	2120922	72.9%

679

680

681 Appendix1 - Table 3. Performance of NextGenMap. Same set of reads was mapped to divergent
 682 genomes. Mapped indicates uniquely mapped reads; proper indicates read with both pairs mapped one
 683 next to the other; mate mapped indicates that both reads in a pair are mapped, although not necessarily
 684 as pairs; singletons indicates the amount of pairs in which only one of both mates was mapped.

%simulated divergence (reference)	total reads	mapped(%)	proper(%)	mate mapped(%)	singletons(%)
-----------------------------------	-------------	-----------	-----------	----------------	---------------

0%	2910370	2873481 (0.99 %)	2869482 (0.99 %)	2872432 (0.99 %)	1049 (0 %)
2%	2910370	2883094 (0.99 %)	2860794 (0.98 %)	2878634 (0.99 %)	4460 (0 %)
4%	2910370	2885714 (0.99 %)	2844842 (0.98 %)	2877808 (0.99 %)	7906 (0.01 %)
6%	2910370	2882035 (0.99 %)	2810920 (0.97 %)	2866362 (0.98 %)	15673 (0.01 %)
8%	2910370	2859215 (0.98 %)	2722782 (0.94 %)	2817502 (0.97 %)	41713 (0.03 %)
10%	2910370	2810639 (0.97 %)	2575954 (0.89 %)	2722242 (0.94 %)	88397 (0.06 %)
12%	2910370	2712723 (0.93 %)	2305232 (0.79 %)	2536014 (0.87 %)	176709 (0.12 %)
14%	2910370	2562495 (0.88 %)	1961916 (0.67 %)	2266582 (0.78 %)	295913 (0.2 %)
16%	2910370	2369165 (0.81 %)	1571078 (0.54 %)	1945446 (0.67 %)	423719 (0.29 %)
18%	2910370	2144444 (0.74 %)	1193318 (0.41 %)	1609114 (0.55 %)	535330 (0.37 %)
20%	2910370	1882993 (0.65 %)	844628 (0.29 %)	1265102 (0.43 %)	617891 (0.42 %)

685

686

687

688 Weichun Huang, Leping Li, Jason R Myers, and Gabor T Marth. ART: a next-generation sequencing read
689 simulator, *Bioinformatics* (2012) 28 (4): 593-594

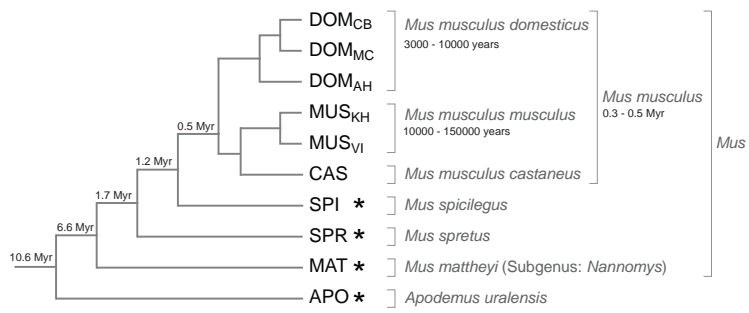
690

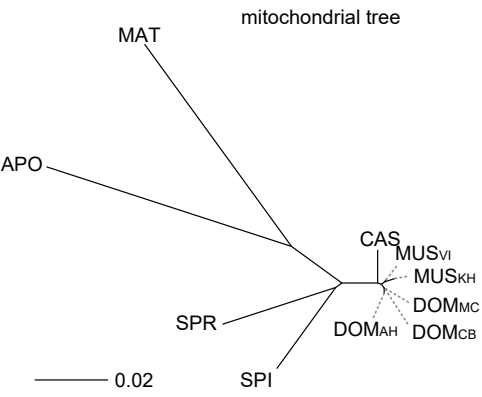
691

692

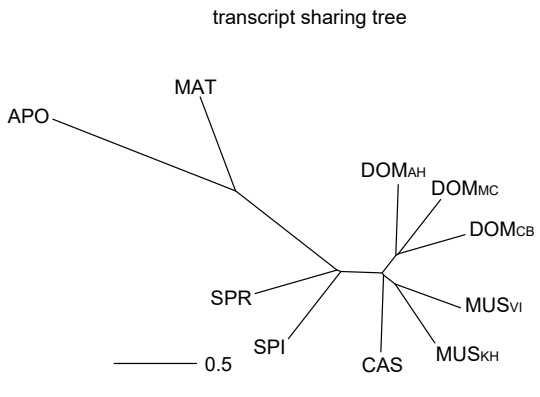
693

694

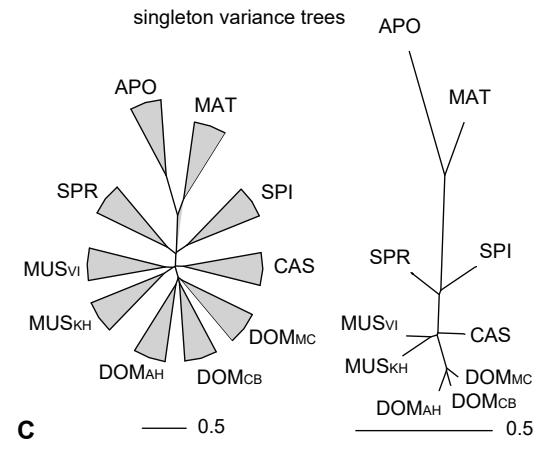




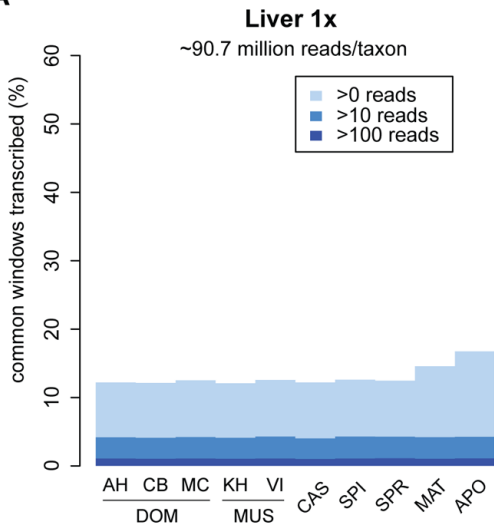
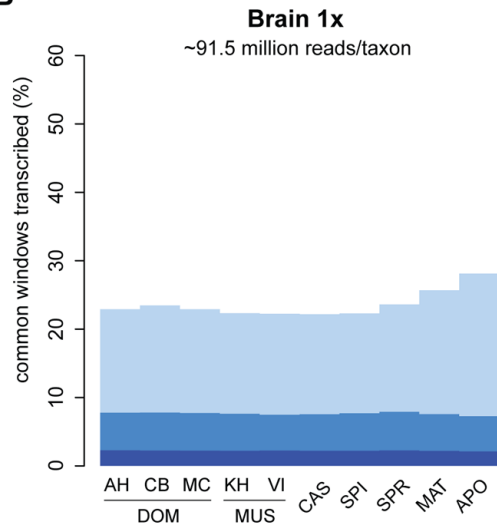
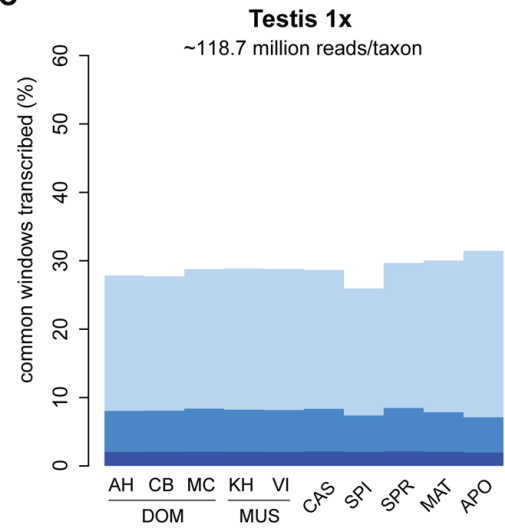
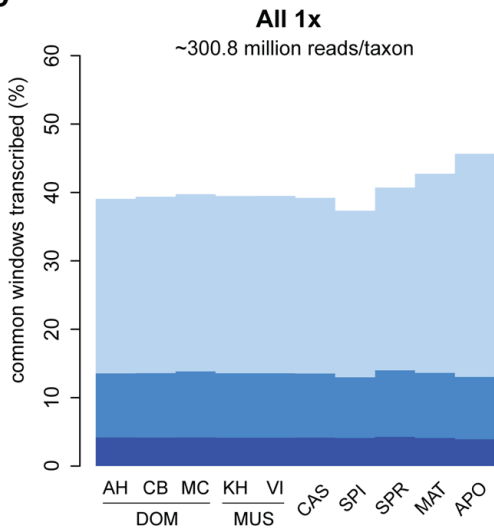
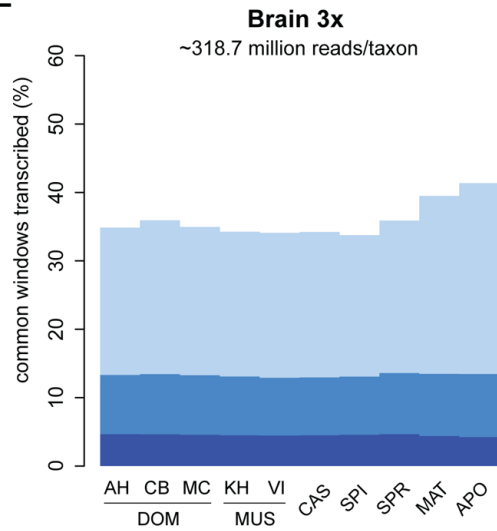
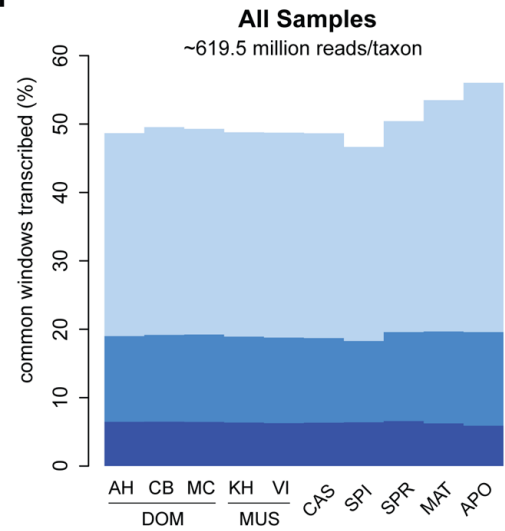
A

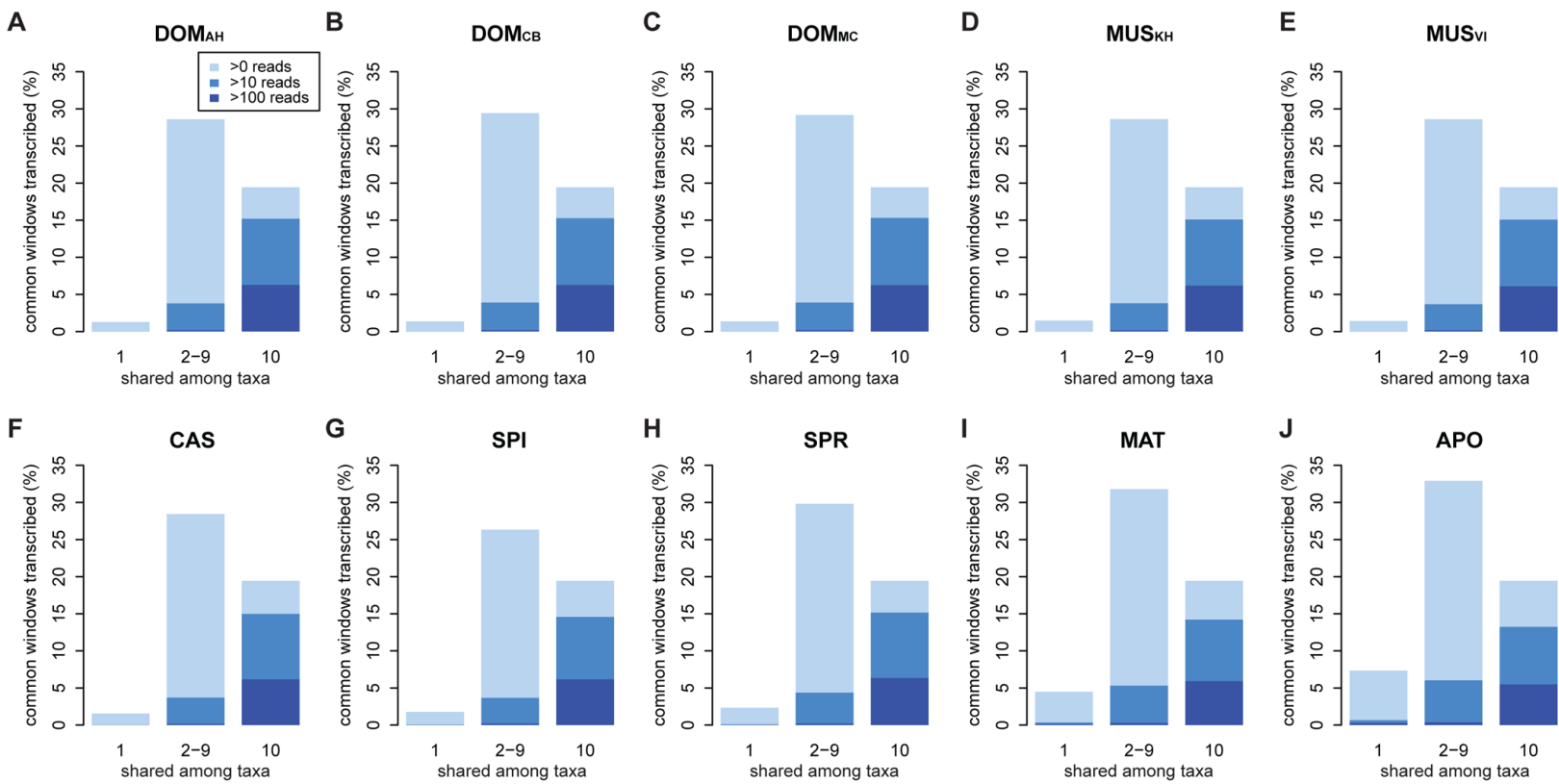


B



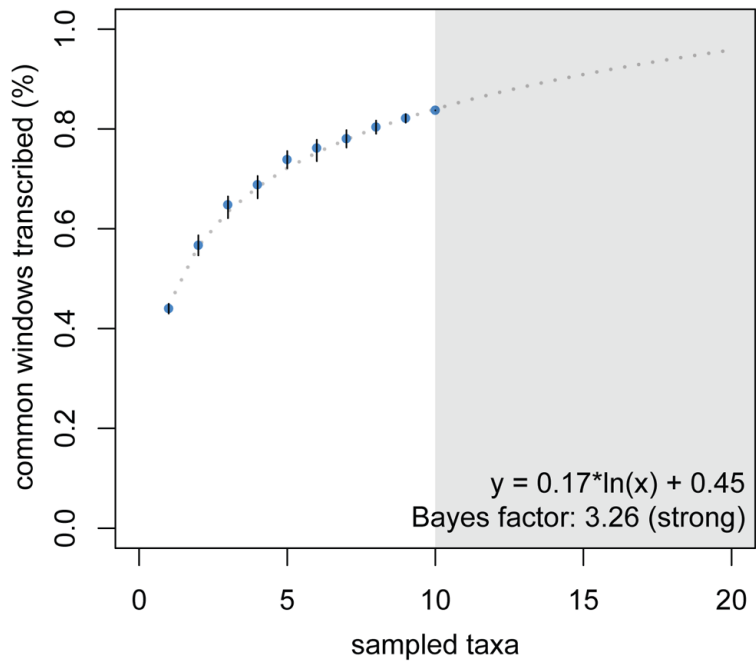
C

A**B****C****D****E****F**

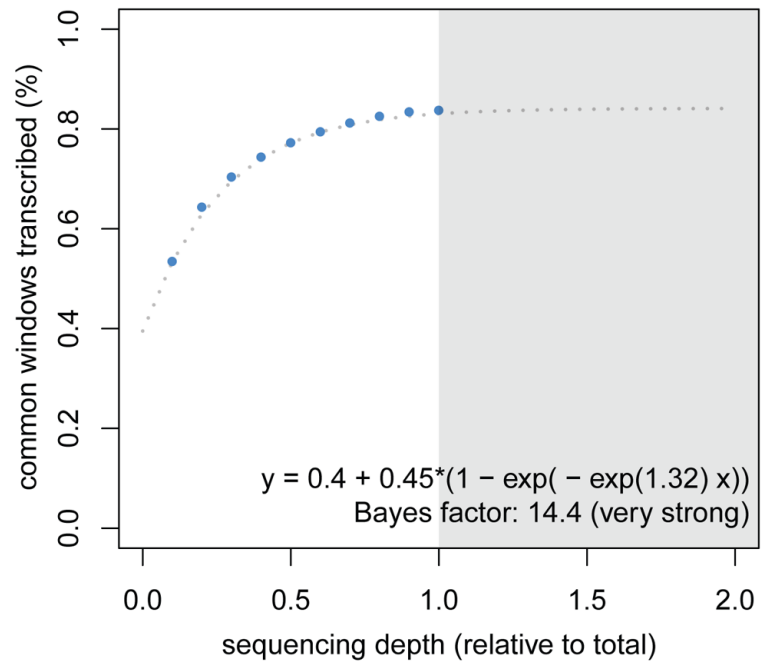


A

saturation species

**B**

saturation sample



Distribution of transcribed
and non-transcribed regions

